Int. J. Nonlinear Anal. Appl. 12 (2021) No. 2, 1267-1287
ISSN: 2008-6822 (electronic)
http://dx.doi.org/10.22075/ijnaa.2020.18958.2045

Viscous dissipation and thermal radiation effects on the flow of Maxwell nanofluid over a stretching surface

G. Narender[a,*], K. Govardhan[b], G. Sreedhar Sarma[a]

[a]Department of H&S (Mathematics), CVR College of Engineering, Hyderabad, Telangana State, India
[b]Department of Mathematics, GITAM University Hyderabad Campus, Telangana State, India

(Communicated by Abdolrahman Razani)

Abstract

An analysis is made to examine the viscous dissipation and thermal effects on magneto hydrodynamic mixed convection stagnation point flow of Maxwell nanofluid passing over a stretching surface. The governing partial differential equations are transformed into a system of ordinary differential equations by utilizing similarity transformations. An effective shooting technique of Newton is utilize to solve the obtained ordinary differential equations. Furthermore, we compared our results with the existing results for especial cases. which are in an excellent agreement. The effects of sundry parameters on the velocity, temperature and concentration distributions are examined and presented in the graphical form. These non-dimensional parameters are the velocity ratio parameter (A), Biot number (Bi), Lewis number (Le), magnetic parameter (M), heat generation/absorption coefficients (A^*, B^*), visco-elastic parameters (β), Prandtl number (Pr), Brownian motion parameter (Nb), Eckert number (Ec), Radiation parameter (R) and local Grashof number (Gc; Gr).

Keywords: Maxwell Nanofluid, Viscous dissipation, Prandtl number, Velocity ratio parameter, Adam's-Moultan Method
2010 MSC: 65M25, 76D05.

1. Introduction

During the past few years, investigating the stagnation point flow of nanofluids has become more popular among the researchers. Nanofluids are formed by the suspension of the nanoparticles in

*Corresponding author
Email addresses: gnriimc@gmail.com (G. Narender), govardhan_kmtm@yahoo.co.in (K. Govardhan), sarma.sreedhar@gmail.com (G. Sreedhar Sarma)

Received: October 2019 *Accepted:* March 2020

conventional base fluids. Examples of such fluids are water, oil or other liquids. The nanoparticles conventionally made up of carbon nanotubes, carbides, oxides or metals, are used in the nanofluids. Keen interest has been taken by many researchers in the nanofluids as compared to the other fluids because of their significant role in industry, medical field and a number of other useful areas of science and technology. Some prominent applications of these fluids are found in magnetic cell separation, paper production, glass blowing, cooling the electronic devices by the cooling pad during the excessive use, etc. Choi [1] introduced the idea of nanofluids for improving the heat transfer potential of the conventional fluids. He experimentally concluded with an evidence that injection of these particles helps in improving the fluid's thermal conductivity. This conclusion opened the best approach to utilize such fluids in mechanical engineering, chemical engineering, pharmaceuticals and numerous different fields. Buongiorno [2], Kuznetsov and Nield [3] followed him and extended the investigation. They worked on the effects of Brownion motion in convactive transport of nanofluids and the investigation of natural convactive transport of nanofluids passing over a vertical surface in a situation when nanoparticles are dynamically controlled at the boundary. Khan and Pop [4] used this concept to evaluate the laminar boundary layer flow, nanoparticles fraction and heat transfer for nanofluids passing over a stretching surface. Zheng et al. [5] explored the effects of radiation on the flow and heat transfer of nanofluids past a stretched surface with temperature jump and velocity slip in a porous media. Impact of radiation upon the heat and mass transfer of the fluids is of remarkable consideration at high operating temperature. In the fluid of engineering, many procedures are executed at high temperature. In such situations, the analysis of the radiation heat transfer plays a key role for the selection of an appropriate equipment. Examples of such fields are atomic and nuclear power plants, artificial satellites, the gas turbines, aircraft industry, missiles manufacturing and wind-turbines etc. Takhar et al. [6] examined the impact of radiation on the magnetohydrodynamic free convection spill for non-gray gas over a semi-infinite plumb surface. Ghaly and Elbarbary [7] delineated the consequences of radiation on the free convection flow of a gas under the MHD effect across a stretching surface with uniform free stream. Devi and Kayalvizhi [8] delivered the analytical solution of MHD flow with radiation passing over a stretching sheet in a porous medium. In industrial sector and modern technology, the non-Newtonian fluids play a vital role.

Non-Newtonian fluids have some interesting applications as they are used in the manufacturing of sports shoes, flexible military suits and viscous coupling. Rising inception of the non-Newtonian fluids like emulsions, molten plastic pulp, petrol and many other chemicals has triggered an appreciable interest in the study of the behavior of such fluids during motion. The mathematical solutions of the models involving the non-Newtonian fluids, are quite interesting and physically applicable. Makinde [9] investigated the buoyancy effect on magnetohydrodynamic stagnation point flow and heat transfer of nanofluids passing over a convectively heated stretching/shrinking sheet. The MHD flow characteristics of a viscoelastic fluid passing over a stretched surface, were studied by Andersson [10]. Later, this work was extended by M. I. Char [11] by including an analysis of the mass transfer. Second order incompressible fluid flows were examined by Marcovitz and Coleman [12]. Rajagopal [13] investigated the unsteady and undirectional flow of a non-Newtonian fluid. Later, Rajagopal and Gupta [14] presented an exact solution of a mathematical model describing the flow of non-Newtonian fluid passing over a porous infinite plate. Siddique et al [15] employed the hodograph trans- formation technique for the mathematical investigation of the flow of non-Newtonian fluid. Some inverse solutions of the non-Newtonian fluid models were worked out by Siddiqui and Kaloni [16]. Chandna and Nguyen [17] used the hodograph transformation technique to get the solution of the non-Newtonian MHD transverse fluid flow problems. Non-Newtonian fluids flows with MHD effects across the orthogonal steady plane were examined by Nguyen and Chandna [18]. The MHD

fluid passing over a stretched sheet, through the porous media with the thermal radiation and the thermal conductivity was examined by Cortell [19].

Bhatta et al. [20] observed the unsteady squeezing nanofluid flow based on water between two disks held parallel to each other in the presence of slip impact. It was observed that an increase in Lewis number decelerate the nano particle concentration. Farooq et al. [21] presented the melting heat transfer effect in the squeezing flow of nanofluid over a Darcy porous medium. They analyzed that the temperature distribution increases for the dominating values of thermophoresis parameter. Gholinia et al. [22] analyzed the different physical impacts such as slip flow and magnetic field on Eyring-Powell fluid along with the homogenous-heterogenous reactions due to rotating disk and conclude that temperature profile is decreased with increasing Pr increased with increasing Nt.G.Narender et al. [23] examined the heat transfer in the nanofluid flow along with the viscous dissipation.

Our prime objective is, we provide the detailed review of Ibrahim and Haq [24]. The numerical results in [24], were acquired by using bvp4c. We reproduce the same results by Adams -Bashforth Moulton fourth order method and additionally by the shooting method. We have extended the flow model of [24], scrutinize the viscous dissipation and thermal radiation effects on the MHD mixed convection stagnation point flow of Maxwell nanofluid over a stretching surface.

2. Problem formulation

We consider the magnetohydrodynamic boundary layer flow of Maxwell nanofluid near the stagnation point over a stretching surface with mixed convection. The coordinates system has been chosen in such a way that $x-$axis is in the direction of the stretching surface and $y-$ axis is in the direction normal to the surface.

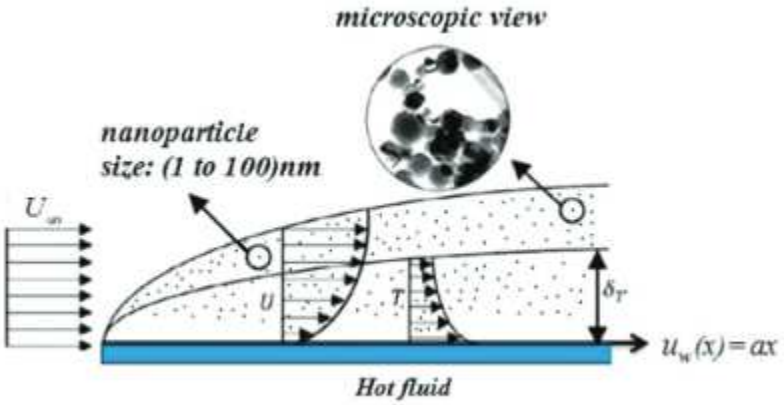

Figure 1: Geometry for the flow under consideration.

Assume that there isn't any flux of nanoparticles at surface. The impact of the thermophoresis has been considered in the boundary conditions. At the surface, the velocity of stretching surface is $u_w(x) = ax$, where "a" is some constant. The flow is directed to a transverse magnetic field B_0 which is supposed to be applied in the direction of positive $y-$axis, perpendicular to the surface. Extending the idea of Ibrahim and Haq. [24], the governing PDEs of the MHD mixed convection stagnation point flow of Maxwell nanofluid along with the viscous dissipation, chemical reaction, thermal radiation parameter and non-uniform internal heat source effects can be written as

Continuity equation

Physical principal: Mass is conserved

$$\frac{\partial u}{\partial x}+\frac{\partial v}{\partial y}=0, \tag{2.1}$$

Momentum equation

Physical principle: $F=ma$

$$u\frac{\partial u}{\partial x}+v\frac{\partial v}{\partial y}=\nu\frac{\partial^2 u}{\partial y^2}+U_\infty\frac{\partial U_\infty}{\partial x}+\frac{sB_0^2(x)}{\rho_f}(U_\infty-u)+\lambda\left[u^2\frac{\partial^2 u}{\partial x^2}+v^2\frac{\partial^2 u}{\partial y^2}+2uv\frac{\partial^2 u}{\partial x\partial y}\right]+$$
$$\beta_T g(T-T_\infty)-\beta_c g(C-C_\infty), \tag{2.2}$$

In equation (2.2). u is the velocity components along x direction and v represent velocity components along the y directions respectively, p the fluid pressure, ρ_f the nanofluid density, ρ_p the density of the particles, v the kinematic viscosity of the base fluid.

Energy equation

Physical principle: Energy is conserved

By using the boundary layer approximations, the boundary layer equation of energy for fluid temperature T is

$$u\frac{\partial T}{\partial x}+v\frac{\partial T}{\partial y}=\alpha\frac{\partial^2 T}{\partial y^2}+t\left(D_B\left(\frac{\partial T}{\partial y}\frac{\partial C}{\partial y}\right)+\left(\frac{D_T}{T_\infty}\right)\left(\frac{\partial T}{\partial y}\right)^2\right)+\frac{\mu}{(\rho c)_p}\left[\left(\frac{\partial u}{\partial y}\right)^2\right]+\frac{q'''}{(\rho c)_p}-\frac{1}{(\rho c)_f}\frac{\partial q_r}{\partial y}, \tag{2.3}$$

Mass transfer equation

$$u\frac{\partial \mathrm{C}}{\partial \mathrm{x}}+\mathrm{v}\frac{\partial \mathrm{C}}{\partial \mathrm{y}}=D_B\left(\frac{\partial \mathrm{C}}{\partial \mathrm{y}}\right)^2+\left(\frac{D_T}{T_\infty}\right)\frac{\partial^2 T}{\partial y^2}-K_1(C-C_\infty), \tag{2.4}$$

In above equations, T is the temperature of the nanofluids and the ambient temperature is T_∞ respectively. C is nanoparticles concentration, C_∞ shows the free stream concentration. Brownian diffusion coefficient D_B, D_T denotes the thermophoretic diffusion coefficient.

Where, q''' represents the temperature and space dependent heat generation and

$$q'''=\frac{Ku_w(x)}{x\ v}\left\{A^*(T_f-T_\infty)f'+B*(T-T_\infty)\right\}$$

where A^* is space dependent and B^* is temperature dependent heat generation. It is observed that $A^*<0$ and $B^*<0$ mean heat absorption whereas in opposite case they communicate generation. In equation (2.4), $K_1(C-C_\infty)$ denotes the chemical reaction term, where K_1 is the chemical reaction parameter.

The associated boundary conditions for the above system of equations are,

$$\left.\begin{array}{llll} u=u_w=ax, & v=0, & -k\frac{\partial T}{\partial y}=h_f(T_f-T), & D_B\frac{\partial C}{\partial y}+\frac{D_T}{T_\infty}\frac{\partial T}{\partial y}=0 \text{ at } y=0, \\ u\to U_\infty=bx, & v=0, & T\to T_\infty, & C\to C_\infty \text{ as } y\to\infty \end{array}\right\} \tag{2.5}$$

The radiative heat flux q_r is given as

$$q_r=\frac{-4\sigma^*}{3k^*}\frac{\partial T^4}{\partial y} \tag{2.6}$$

where σ^* and k^* stand for the Stefan-Boltzmann constant and coefficient of mean absorption, and T^4 is the linear sum of temperature and it can expand with the help of Taylor series along with T_∞

$$T^4=T_\infty^4+4T_\infty^3(T-T_\infty)+6T_\infty^2(T-T_\infty)^2+\ldots \tag{2.7}$$

Ignoring the terms with higher order in $(T - T_\infty)$, we get

$$T^4 = 4T_\infty^3 T - 3T_\infty^4 \tag{2.8}$$

substituting (2.8) into (2.6), we get

$$q_r = \frac{-16T_\infty^3\sigma^*}{3k^*}\frac{\partial T}{\partial y} \tag{2.9}$$

3. Dimensionless form of the model

To convert the PDEs (2.1)-(2.4) along with the BCs (2.5) into the dimensionless form, we use the similarity transformation [20]:

$$\eta = y\sqrt{\frac{c}{\nu}}, \quad \psi = \sqrt{c\nu}xf(\eta), \quad \theta(\eta) = \frac{T - T_\infty}{T_f - T_\infty}, \quad \phi(\eta) = \frac{C - C_\infty}{C_w - C_\infty}. \tag{3.1}$$

In above, $\psi(x, y)$ denotes stream function obeying

$$u = \frac{\psi}{\partial y}, \quad \nu = -\frac{\psi}{\partial x} \tag{3.2}$$

The equation of continuity (2.1) is satisfied identically. The governing equations (2.2)- (2.4) are reduced into the following nonlinear ODEs:

$$f''' + ff'' - f'^2 - A^2 + M(A - f') + \beta\left(f^2 f''' - 2ff'f''\right) + Gr\theta + Gc\phi = 0, \tag{3.3}$$

$$\left(1 + \frac{4}{3}R\right)\theta'' + Pr\left(f\theta' + Nb\theta'\beta' + Nt\theta'^2 + Ecf''^2\right) + A^*f' + B^*\theta = 0, \tag{3.4}$$

$$\phi'' + Le\ Pr\ f\ \phi' + \frac{Nt}{Nb}\theta'' - \chi\ Le\,\mathrm{Pr}\,\phi = 0. \tag{3.5}$$

The associated boundary conditions (2.5) get the form:

$$f(0) = 0, \quad f'(0) = 1, \quad \theta'(0) = -Bi\left[1 - \theta(0)\right], \quad Nb\beta'(0) + Nt'(0) = 0, \text{ at } \eta = 0, \tag{3.6}$$

$$f'(\infty) \to A, \quad \theta(\infty) \to 0, \quad \beta(\infty) \to 0 \text{ as } \eta \to \infty \tag{3.7}$$

Different parameters used in the above equations have the following formulations:

$$\left.\begin{array}{c} Gr = \frac{g\beta_T}{a^2x}(T_f - T), \quad Gc = \frac{g\beta_C}{a^2x}C_\infty, \quad LePr = Sc = \frac{\nu}{D_B}, \\ A = \frac{b}{a}, \quad Pr = \frac{\mu C_p}{K}, \quad \chi = \frac{K_1}{a}, \quad \beta = \lambda a, \quad M = \frac{\sigma B_0^2}{\rho_f a}, \\ Nb = \frac{(\rho c)_p D_B C_\infty}{(\rho c)_f \nu}, \quad Nb = \frac{(\rho c)_p D_T\left(T_f - T\right)}{(\rho c)_f \nu T_\infty}, \quad Ec = \frac{u_w^2}{\left[(C_p)_f (T_w - T_\infty)\right]}, \quad R = \frac{-4T_\infty^3\sigma^*}{3k^*k} \end{array}\right\} \tag{3.8}$$

In this problem, the desired physical quantities are the local Nusselt number Nu_x and the skin-friction coefficient C_f. These quantities are defined as

$$C_f = \frac{t_w}{\rho u_w^2}, \quad Nu_x = \frac{xq_w}{k((T_w - T_\infty)} \tag{3.9}$$

Here, the wall heat flux q_w and the wall shear stress t_w are given as

$$t_w = \mu\left(\frac{\partial u}{\partial y}\right)_{y=0}, \quad q_w = -k\left(\frac{\partial T}{\partial y}\right)_{y=0} \tag{3.10}$$

With the help of above equations, we get

$$C_f\sqrt{Re_x} = -f''(0), \quad \frac{Nu_x}{\sqrt{Re_x}} = -\theta'(0) \tag{3.11}$$

where $R_x = \frac{ax^2}{\nu}$ is the local Reynolds number.

4. Numerical results

In this Section, the scheme for the numerical solution of the system of three coupled ODEs (3.3)-(3.5) with BCs (3.6)-(3.7) will be discussed. Because of its efficiency, the shooting technique has been preferred to apply. First, the system of equations (3.3)-(3.5) will be transmuted into a system of ODEs. We can write

$$f''' = \frac{1}{1+\beta f^2}\left[-ff'' + f'^2 - A^2 - M(A-f') + 2\beta ff'f'' - Gr\theta - Gc\phi\right] \tag{4.1}$$

$$\theta'' = \frac{-Pr}{\left(1+\frac{4}{3}R\right)}\left(f\theta' + Nb\theta'\beta' + Nt\theta'^2 + Ecf''^2\right) - A^*f' - B^*\theta \tag{4.2}$$

$$\phi'' = -Le\ Pr\ \ f\ \phi' - \frac{Nt}{Nb}\theta'' + \chi\ Le\mathrm{Pr}\,\phi = 0 \tag{4.3}$$

By using the following notations

$$f = y_1, \quad f' = y_2, \quad f'' = y_3, \quad \theta = \ y_4, \quad \theta' = y_5, \quad \phi = y_6, \quad \phi' = y_7 \tag{4.4}$$

the above system of coupled nonlinear ODEs is converted into the following system of seven first order equations:

$$\begin{aligned}
y_1' &= y_2,\\
y_2' &= y_3,\\
y_3' &= \frac{1}{1+\beta y_1^2}\left[-y_1y_3 + y_2^2 - A^2 - M(A-y_2) + 2\beta y_1y_2y_3 - Gry_4 - Gcy_6\right],\\
y_4' &= y_5,\\
y_5' &= \frac{-Pr}{1+\frac{4}{3}R}\left[y_1y_5 + Nby_1y_7 + Nty_5^2 + Ecy_3^2\right] - A^*y_2 - B^*y_4\\
y_6' &= y_7,\\
y_7' &= -Le\ Pr\ y_1y_7 - \frac{Nt}{Nb}y_5' + \chi Pry_6
\end{aligned}$$

The resulting form of the boundary conditions is

$$y_1(0) = 0,\ y_2(0) = 1,\ y_5(0) = Bi\,(\,y_4(0) - 1),\ y_7(0) = -\frac{Nt}{Nb}y_5(0),$$

$$y_2 \to A,\ y_4 \to 0,\ y_6 \to 0 \text{ as } \eta \to \infty$$

To execute the numerical procedure, the unbounded domain $[0, \infty)$ has been replaced by $[0, \eta_{max}]$ for some suitable choice of η_{max}. An asymptotic convergence of the numerical solution is observed by increasing the value of η_{max}. The above initial value problem will be solved by Adams-Bashforth-Moulton Method of order four. The shooting method requires some initial guess for $y_3(\eta)$, $y_4(\eta)$

and $y_6(\eta)$ at $\eta = 0$. The initial guess are updated by the Newton's method until a solution of the problem which approximately meets the given boundary conditions at the right end of the domain.

In order to validate the code adopted for the numerical solution of equations governing the natural convective flow, the comparison of current results with some of the earlier published work on free convection [24] are displayed in Table 1 and Table 2. Excellent agreement of current results with those previously published results encourage us to use the present code. The physical parameters, the local skin-friction coefficient C_f and the local Nusselt number Nu_x, are of great interest for engineers and mathematicians. The skin-friction coefficient examines the viscous stress acting on the surface of the body whereas the local Nusselt number Nu_x is the ratio between the convective heat transfer and the conductive heat transfer at the surface of the body.

Table 1: Numerical results of $-f''(0)$ and $-\theta''(0)$ for different values of A, M, β, χ, Le and Bi with $Gr = Gc = 0.1$, $Pr = 1.0$, $Nb = Nt = 0.3$, $A^* = 0.4$, $B^* = 0.7$

A	**M**	β	χ	**L**e	**B**i	$-f''(0)$		$-\theta''(0)$	
						[24]	Present Results	[24]	Present Results
0.1	0.1	0.6	0.6	0.2	0.2	1.243941	1.243942000	0.325186	0.325186000
0.2						1.189946	1.189947000	0.591051	0.591053700
0.3						1.242064	1.242061000	1.484108	1.484087000
	0.5					1.084907	1.084908000	0.395633	0.395631100
	1.0					1.243941	1.243942000	0.325186	0.325185600
	1.5					1.390760	1.390761000	0.288612	0.288611700
		0.4				1.277225	1.277225000	0.304179	0.304180400
		0.6				1.243941	1.243942000	0.325186	0.325185700
		0.8				1.211603	1.211604000	0.351818	0.351817700
			0.0			1.227885	1.227886000	0.331895	0.331895900
			0.6			1.243941	1.243942000	0.325186	0.325185600
			0.9			1.247504	1.247505000	0.323943	0.323943900
				0.2		1.243941	1.243942000	0.325186	0.325185600
				0.6		1.254848	1.254848000	0.321263	0.321263200
				1.0		1.258224	1.258224000	0.321617	0.321617400
					0.1	1.240617	1.240617000	0.165669	0.165670200
					0.2	1.243941	1.243942000	0.325186	0.325185600
					0.3	1.247096	1.247097000	0.478489	0.478490400

Table 1 and 2 include the numerical values of C_f and Nu_x denoted by $-f''(0)$ and $-\theta''(0)$ respectively, for different physical parameters. It is observed that increasing the values of the magnetic parameter, thermal Grashof number, Brownian motion parameter, space dependent heat generation/absorption coefficient, chemical reaction parameter, Lewis number, Biot number, enhances the local skin-friction coefficient. Furthermore, the skin friction coefficient decreases by enlarging the values of viscoelastic parameter, solutal Grashof number, thermophoresis parameter, time dependent heat generation/absorption coefficient, whereas it shows a mixed behavior by increasing the velocity ratio parameter and Prandtl number. The Nusselt number shows an increasing behavior for the velocity ratio parameter, the viscoelastic parameter, the solutal Grashof number, the thermophoresis parameter, the space dependent heat generation/absorption coefficient and the Biot number. It shows a decreasing behavior for the magnetic parameter, the thermal Grashof number, the Brownian motion parameter, the time dependent heat generation/absorption coefficient and the chemical

Table 2: Numerical results of $-f''(0)$ and $-\theta''(0)$ for different values of Gr, Gc, Pr, Nb, Nt, A^* and B^* with $A = 0.1, M = 1.0, \beta = \chi = 0.6$, $Le = Bi = 0.2$.

Gr	**G**c	**P**r	**N**b	**N**t	A^*	B^*	$-f''(0)$		$-\theta''(0)$	
							[24]	Present Results	[24]	Present Results
0.1	0.1	1.0	0.3	0.3	0.4	0.7	1.243941	1.243942000	0.325186	0.325185600
0.0							1.179313	1.179314000	0.405135	0.405134600
0.1							1.243941	1.243942000	0.325186	0.325185600
0.2							1.278005	1.278006000	0.284902	0.284902800
	0.1						1.243941	1.243942000	0.325186	0.325185600
	0.2						1.224684	1.224685000	0.342247	0.342247700
	0.3						1.201199	1.201200000	0.361681	0.361682400
		1.0					1.243941	1.243942000	0.325186	0.325185600
		3.0					1.185067	1.185067000	0.075197	0.075197930
		5.0					1.197508	1.197509000	0.131813	0.131813700
			0.3				1.243941	1.243942000	0.325186	0.325185600
			0.5				1.250604	1.250605000	0.318870	0.318870000
			0.7				1.253289	1.253290000	0.316238	0.316238600
				0.0			1.255546	1.255547000	0.297469	0.297469700
				0.1			1.252189	1.252191000	0.305726	0.305726200
				0.3			1.243941	1.243942000	0.325186	0.325185700
					0.1		1.222541	1.222542000	0.232237	0.232237200
					0.2		1.230012	1.230013000	0.264929	0.264929900
					0.4		1.243941	1.243942000	0.325186	0.325186100
						0.7	1.243941	1.243942000	0.325186	0.325186100
						0.8	1.232713	1.232714000	0.271875	0.271875800
						0.9	1.225808	1.225810000	0.237573	0.237573900

reaction parameter. It is also noticed that the Nusselt number shows a mixed behavior for Prandtl number and Lewis number.

5. Graphical results

The objective is to inspect governing parameters on the velocity, temperature and concentration distribution in this Section.

5.1. Velocity ratio parameter

Figure 2 designates that by increasing the value of A ($A > 1$), the thickness of hydrodynamic boundary layer increases, and it decreases by decreasing the value of A ($A < 1$). Physically, when the free stream velocity is more than the stretching velocity, the ratio between the free stream velocity and the stretching velocity is greater than 1, consequently, it decline the retarding force and increase the flow velocity. The impact of velocity ratio on the temperature $\theta(\eta)$ has been highlighted by Figure 3. As the value of the velocity ratio is increased, the temperature of the surface decreases at the surface and furthermore, the thickness of thermal boundary layer declines. Figure 4 demonstrates the concentration profile $\phi(\eta)$ under the influence of the velocity ratio parameter. It has the decreasing effects on the concentration profile near the wall. It increases a little bit away from the wall and a little further away from the wall it starts decreasing again.

5.2. Magnetic Parameter

Figure 5 depicts the impact of M on the dimensionless velocity $f^{'}$. Here, by increasing the value of M, velocity profile gets declines. Figure 6 describes the impact of M on the temperature profile. It is shown in Figure 5.6 that by increasing the value of the magnetic parameter, temperature profile $\theta(\eta)$ gets increase. The impact of the magnetic parameter on the dimensionless concentration, is presented in Figure 7. The concentration profile is found to increase when the magnetic parameter increases near the surface. It decreases a bit away from the surface and interestingly, it again starts increasing a bit further away from the surface.

5.3. Prandtl number

The temperature profile decreases with increasing Prandtl number as depicted in Figure 8. The effect of the variation in the Pr on the concentration profile, is observed in Figure 9. It is notified from the figure, as the value of Prandtl number rises, the nanoparticles scattered out toward the outward, consequently, the nanoparticles concentration at the surface decreases.

5.4. Brownian motion parameter

The impact of Brownian motion parameter is witness in Figure 10 that concentration profile increases by increasing the Nb. Consequently, the Brownian force increases the nanoparticle concentration at the surface. Thus, the concentration profile increases on the surface, but it is found to decrease a bit away from the surface.

5.5. Thermophoresis Parameter

Through Figure 11, it can be noticed that by enlarging the thermophoresis parameter, thickness of boundary layer also increases, which causes an increase in the velocity profile f'. Figure 12 includes the graphs of the temperature distribution in thermal boundary layer for various value of the Nt. It is noticed that if the thermophoesis increases, causing an increase in Nt. Figure 13 describes the influence of the Nt on the concentration profile. Therefore, when the influence of the thermophoretic force is enlarged, the concentration profile on the surface declines, which is the opposite in nature to that of the case of the Brownian motion but a bit away from the wall it starts increasing.

5.6. Lewis number

Similar effects are shown for the temperature profile in Figure 14. The impact of Le on the concentration profile is seen in Figure 15. Increasing the Lewis number, the concentration profile near the surface increases but a bit away from the surface it starts decreasing by enhancing the influence of the Lewis number Le.

5.7. Biot number

Figure 16 show the influence of convective heating, also known as the Biot number Bi, on the temperature distribution respectively. Physically, convective heating Bi can be calculated by dividing the convaction at the surface to the conduction on the surface of a body. As an impact of the increasing the Bi, the temperature on the surface increase, which results thickening of the thermal boundary layer, whereas the Biot number causes a decrease in the concentration profile ϕ, which is indeed reflected in Figure 17.

5.8. Viscoelastic parameter

It is noticed in Figure 18 that as the viscoelastic parameter increases, which causes an increase in the velocity profile. Figure 19 depicts exactly the opposite effect of viscoelastic parameter on the temperature profile. The impact of the viscoelastic parameter β on the dimensionless concentration is presented in Figure 20. The concentration profile is found to decrease when the viscoelastic parameter increases near the surface. It increases a bit away from the wall and interestingly, it again starts decreasing a bit further away from the surface.

5.9. Space dependent heat generation/absorption coefficient

Figure 21 delineates the effect of the A^* on the temperature. The temperature profile is increased by increasing the value of the space dependent heat generation/absorption coefficient A^*. Effect of the space dependent heat generation/absorption coefficient on the concentration is shown in Figure 22. Initially, concentration profile increases by increasing the space dependent heat generation/absorption coefficient, it starts decreasing a bit away from the surface. Finally, it again increases a bit further away from the surface.

5.10. Temperature dependent heat generation/absorption coefficient

Figure 23 indicates the impact of the temperature dependent heat generation/absorption B^* on the temperature profile. This figure describes that by increasing the temperature dependent heat generation/absorption B^*, temperature profile increases. It is seen from Figure 24 that by increasing the value of the temperature dependent heat generation/absorption, the concentration profile shows an interesting behavior. Initially, near the wall it increases, then decreases a bit away from the wall and again it starts increasing a bit further away from the wall.

5.11. Chemical reaction parameter

Effect of on the concentration is included in Figure 25. The concentration distribution increases with the increasing values of but a bit away from the surface it starts decreasing.

5.12. Solutal Grashof number

The effect of the solutal Grashof number on the velocity profile is presented in Figure 26. Increasing the solutal Grashof number Gc, the velocity profile is observed to increase. Also observed that by increasing the solutal Grashof number, initially, the concentration profile decreases near the surface. It increases a bit away from the surface and then again it starts decreasing a bit further away from the surface.

5.13. Thermal Grashof number

The effect of the Gr on the velocity profile is shown in Figure 27. It is noticed that the thermal Grashof number contributes to increase the velocity profile if all other parameters that appear in the velocity field are kept constant. Figure 28 designates that by increasing the value of the thermal Grashof number, the temperature profile decreases. In Figure 29, the concentration profile shows an interesting behavior for different values of the thermal Grashof number. Figure delineates that by increasing the thermal Grashof number, initially, the concentration profile decreases near the wall. It increases a bit away from the wall and then again it starts decreasing a bit further away from the wall.

5.14. Eckert number

Figure 30 shows that by increasing the Eckert number, the velocity profile increases. Boundary layer decreases. In Figure 31, it indicates that increasing the value of Eckert number Ec has the enhancing effect on temperature profile. The physical reason behind it is that an increment in the dissipation enhances the thermal conductivity of the fluid which causes an enhancement in the thermal boundary layer and increases the thermal boundary layer thickness in the flow field. It is noticed from Figure 5.43 that concentration profiles first decrease near the sheet surface and situation is completely reversed in the other part of the boundary layer flow.

5.15. Radiation parameter

Figure 32 and 33 shows the effect of thermal radiation on temperature and concentration profile respectively. Figure 34 shows the influence of R on the temperature profile. From this graph, by increasing R, the temperature profile is enhanced. Thus, the boundary layer thickness is increased, and also observed by increasing R concentration profile is decreasing.

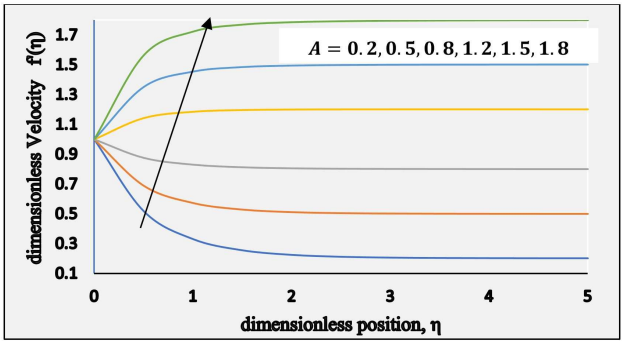

Figure 2: Dimensionless Velocity vs A when $M = 2.5$, $Pr = 2$, $Nb = Nt = 0.5, Le = 5$, $Bi = 5$, $\beta = 0.2$, $A^* = 0.1, B^* = 0.2$, $\chi = 0.5$, $Gr = 0.1, Gc = 0.1$, $Ec = 0.2$ and $R = 0.1$

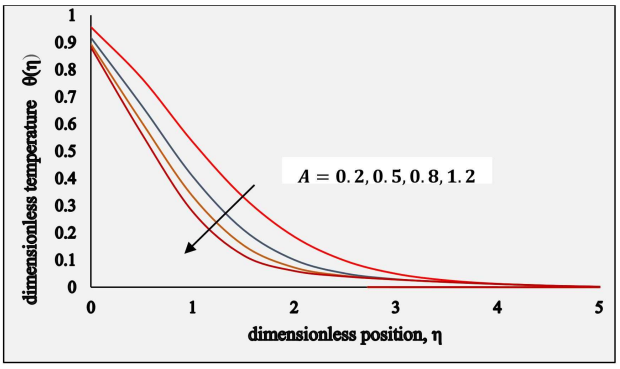

Figure 3: Dimensionless Temperature vs A when $M = 2.5$, $Pr = 2$, $Nb = Nt = 0.5, Le = 5$, $Bi = 5$, $\beta = 0.2$, $A^* = 0.1, B^* = 0.2$, $\chi = 0.5$, $Gr = 0.1, Gc = 0.1$, $Ec = 0.2$ and $R = 0.1$

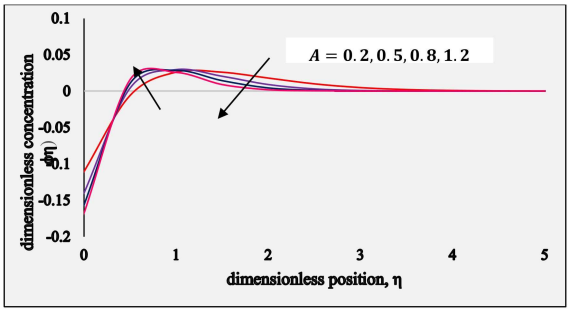

Figure 4: Dimensionless Concentration vs A when $M = 2.5$, $Pr = 2$, $Nb = Nt = 0.5, Le = 5$, $Bi = 5$, $\beta = 0.2$, $A^* = 0.1, B^* = 0.2$, $\chi = 0.5$, $Gr = 0.1, Gc = 0.1$, $Ec = 0.2$ and $R = 0.1$

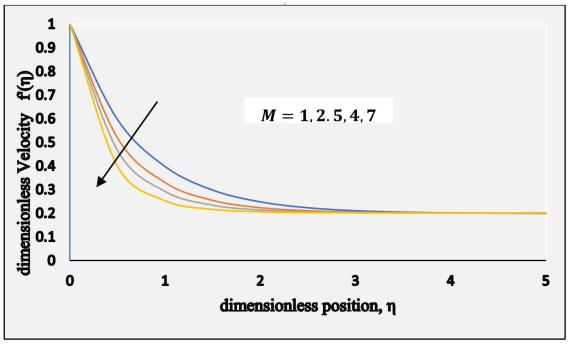

Figure 5: Dimensionless Velocity vs M when $A = 0.2$, $Pr = 2$, $Nb = Nt = 0.5, Le = 5$, $Bi = 5$, $\beta = 0.2$, $A^* = 0.1, B^* = 0.2$, $\chi = 0.5$, $Gr = 0.1, Gc = 0.1$, $Ec = 0.2$ and $R = 0.1$

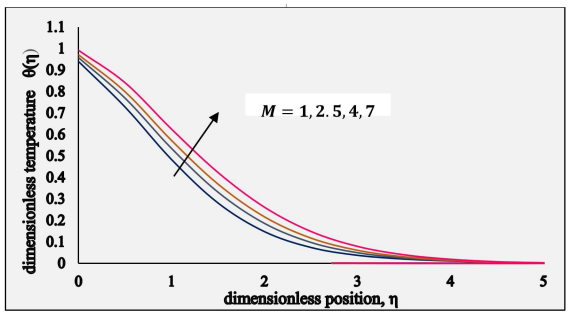

Figure 6: Dimensionless temperature vs M when $A = 0.2$, $Pr = 2$, $Nb = Nt = 0.5, Le = 5$, $Bi = 5$, $\beta = 0.2$, $A^* = 0.1, B^* = 0.2$, $\chi = 0.5$, $Gr = 0.1, Gc = 0.1$, $Ec = 0.2$ and $R = 0.1$

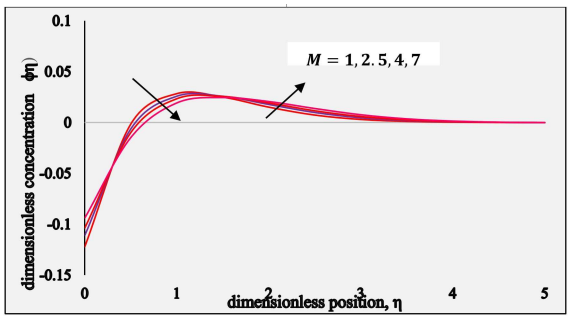

Figure 7: Dimensionless Concentration vs A when $M = 2.5$, $Pr = 2$, $Nb = Nt = 0.5, Le = 5$, $Bi = 5$, $\beta = 0.2$, $A^* = 0.1, B^* = 0.2$, $\chi = 0.5$, $Gr = 0.1, Gc = 0.1$, $Ec = 0.2$ and $R = 0.1$

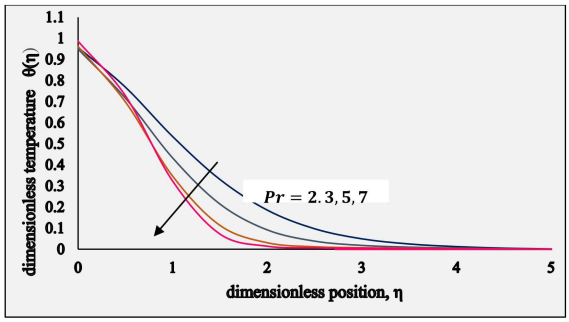

Figure 8: Dimensionless temperature vs Pr when $A = 0.2$, $M = 2.5$, $Nb = Nt = 0.5, Le = 5$, $Bi = 5$, $\beta = 0.2$, $A^* = 0.1, B^* = 0.2$, $\chi = 0.5$, $Gr = 0.1, Gc = 0.1$, $Ec = 0.2$ and $R = 0.1$

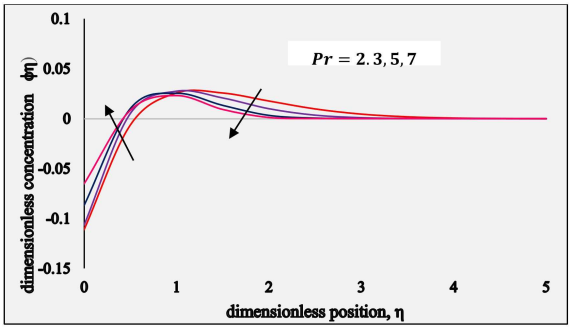

Figure 9: Dimensionless concentration vs Pr when $A = 0.2$, $M = 2.5$, $Nb = Nt = 0.5, Le = 5$, $Bi = 5$, $\beta = 0.2$, $A^* = 0.1, B^* = 0.2$, $\chi = 0.5$, $Gr = 0.1, Gc = 0.1$, $Ec = 0.2$ and $R = 0.1$

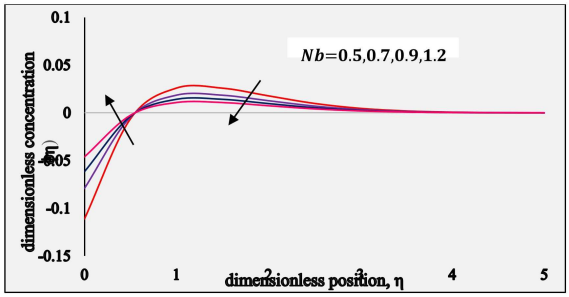

Figure 10: Dimensionless concentration vs Nb when $A = 0.2$, $M = 2.5$, $Pr = 2$, $Nt = 0.5, Le = 5$, $Bi = 5$, $\beta = 0.2$, $A^* = 0.1, B^* = 0.2$, $\chi = 0.5$, $Gr = 0.1, Gc = 0.1$, $Ec = 0.2$ and $R = 0.1$

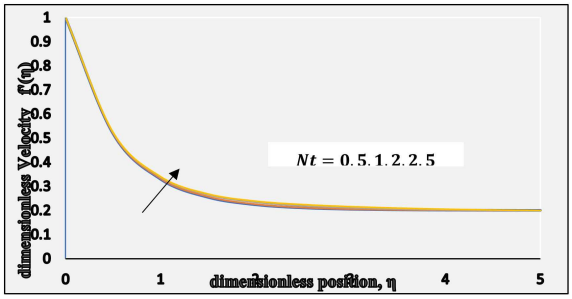

Figure 11: Dimensionless Velocity vs Nt when $A = 0.2$, $M = 2.5$, $Pr = 2$, $Nb = 0.5, Le = 5$, $Bi = 5$, $\beta = 0.2$, $A^* = 0.1, B^* = 0.2$, $\chi = 0.5$, $Gr = 0.1, Gc = 0.1$, $Ec = 0.2$ and $R = 0.1$

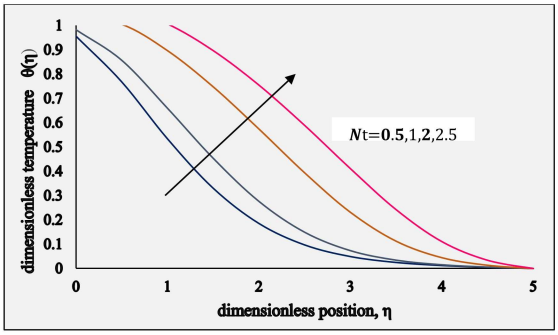

Figure 12: Dimensionless temperature vs Nt when $A = 0.2$, $M = 2.5$, $Pr = 2$, $Nb = 0.5, Le = 5$, $Bi = 5$, $\beta = 0.2$, $A^* = 0.1, B^* = 0.2$, $\chi = 0.5$, $Gr = 0.1, Gc = 0.1$, $Ec = 0.2$ and $R = 0.1$

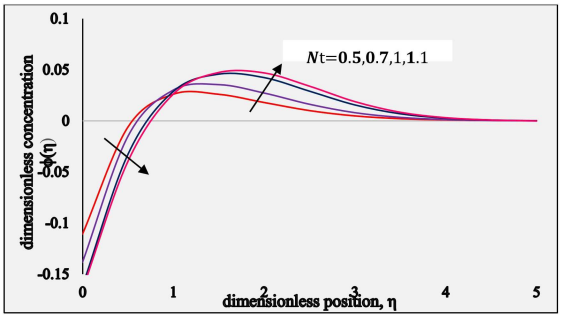

Figure 13: Dimensionless concentration vs Nt when $A = 0.2$, $M = 2.5$, $Pr = 2$, $Nb = 0.5, Le = 5$, $Bi = 5$, $\beta = 0.2$, $A^* = 0.1, B^* = 0.2$, $\chi = 0.5$, $Gr = 0.1, Gc = 0.1$, $Ec = 0.2$ and $R = 0.1$

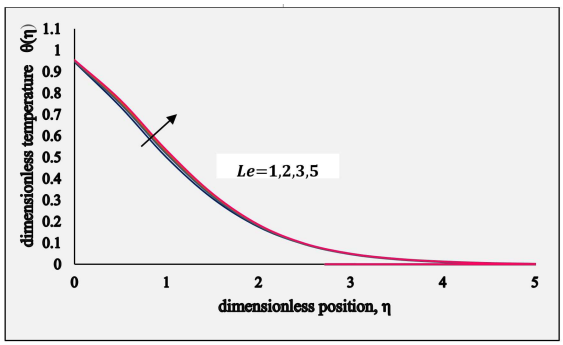

Figure 14: Dimensionless temperature vs Le when $A = 0.2$, $M = 2.5$, $Nb = Nt = 0.5, Pr = 2$, $Bi = 5$, $\beta = 0.2$, $A^* = 0.1, B^* = 0.2$, $\chi = 0.5$, $Gr = 0.1, Gc = 0.1$, $Ec = 0.2$ and $R = 0.1$

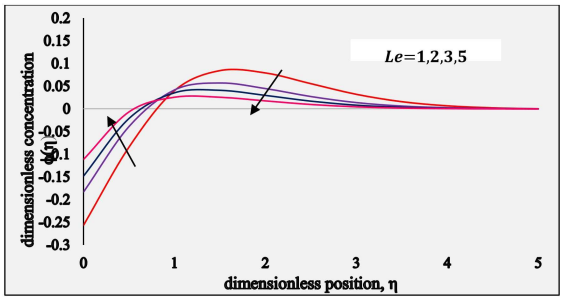

Figure 15: Dimensionless concentration vs Le when $A = 0.2$, $M = 2.5$, $Nb = Nt = 0.5, Pr = 2$, $Bi = 5$, $\beta = 0.2$, $A^* = 0.1, B^* = 0.2$, $\chi = 0.5$, $Gr = 0.1, Gc = 0.1$, $Ec = 0.2$ and $R = 0.1$

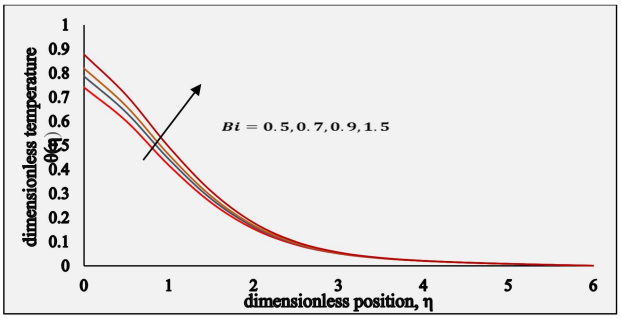

Figure 16: Dimensionless temperature vs Bi when $M = 2.5$, $Pr = 2$, $Nb = Nt = 0.5, Le = 5$, $A = 0.2$, $\beta = 0.2$, $A^* = 0.1, B^* = 0.2$, $\chi = 0.5$, $Gr = 0.1, Gc = 0.1$, $Ec = 0.2$ and $R = 0.1$

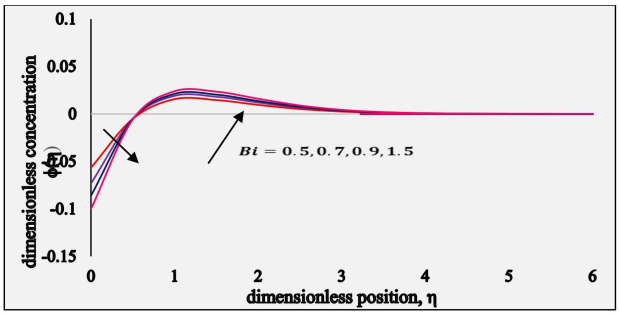

Figure 17: Dimensionless Concentration vs A when $M = 2.5$, $Pr = 2$, $Nb = Nt = 0.5, Le = 5$, $Bi = 5$, $\beta = 0.2$, $A^* = 0.1, B^* = 0.2$, $\chi = 0.5$, $Gr = 0.1, Gc = 0.1$, $Ec = 0.2$ and $R = 0.1$

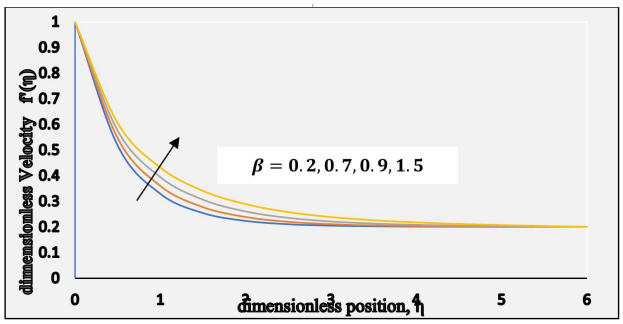

Figure 18: Dimensionless Velocity vs β when $M = 2.5$, $Pr = 2$, $Nb = Nt = 0.5, Le = 5$, $Bi = 5$, $Pr = 2$, $A^* = 0.1, B^* = 0.2$, $\chi = 0.5$, $Gr = 0.1, Gc = 0.1$, $Ec = 0.2$ and $R = 0.1$

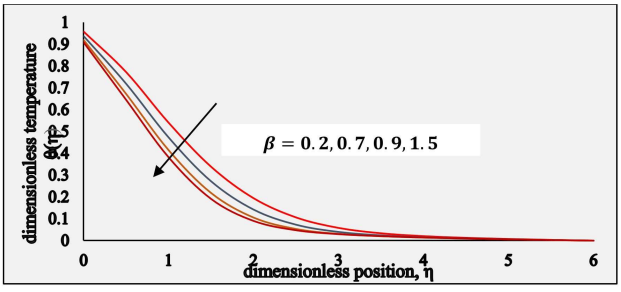

Figure 19: Dimensionless temperature vs β when $M = 2.5$, $Pr = 2$, $Nb = Nt = 0.5, Le = 5$, $Bi = 5$, $Pr = 2$, $A^* = 0.1, B^* = 0.2$, $\chi = 0.5$, $Gr = 0.1, Gc = 0.1$, $Ec = 0.2$ and $R = 0.1$

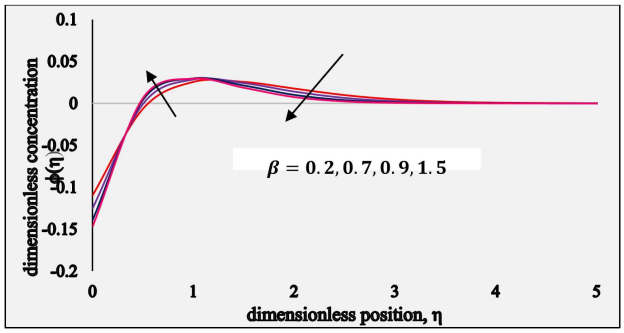

Figure 20: Dimensionless concentation vs β when $M = 2.5$, $Pr = 2$, $Nb = Nt = 0.5, Le = 5$, $Bi = 5$, $Pr = 2$, $A^* = 0.1, B^* = 0.2$, $\chi = 0.5$, $Gr = 0.1, Gc = 0.1$, $Ec = 0.2$ and $R = 0.1$

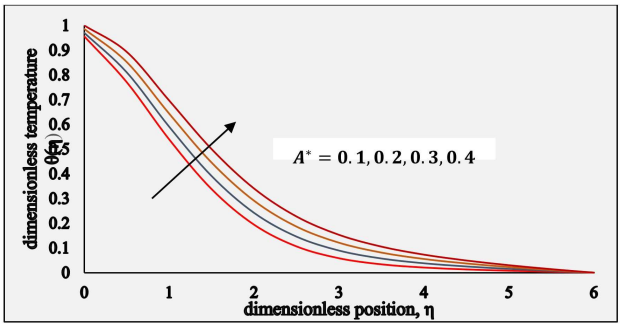

Figure 21: Dimensionless temperature vs $\mathbf{A}^*$ when $M = 2.5$, $Pr = 2$, $Nb = Nt = 0.5, Le = 5$, $Bi = 5$, $Pr = 2$, $\beta = 0.2, B^* = 0.2$, $\chi = 0.5$, $Gr = 0.1, Gc = 0.1$, $Ec = 0.2$ and $R = 0.1$

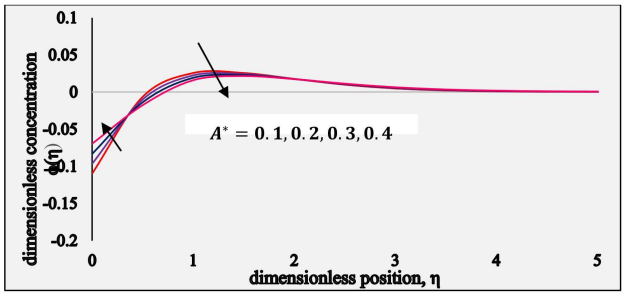

Figure 22: Dimensionless concentration vs $\mathbf{A}^*$ when $M = 2.5$, $Pr = 2$, $Nb = Nt = 0.5, Le = 5$, $Bi = 5$, $Pr = 2$, $\beta = 0.2, B^* = 0.2$, $\chi = 0.5$, $Gr = 0.1, Gc = 0.1$, $Ec = 0.2$ and $R = 0.1$

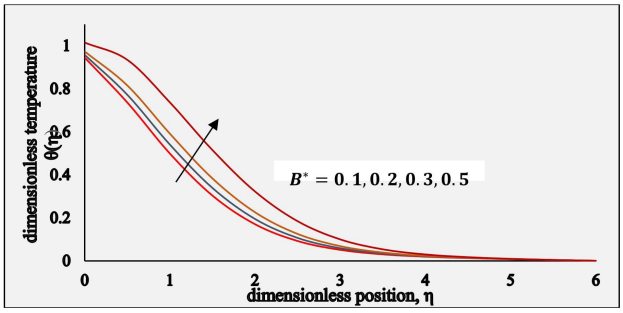

Figure 23: Dimensionless temperature vs B^* when $M = 2.5$, $Pr = 2$, $Nb = Nt = 0.5, Le = 5$, $Bi = 5$, $Pr = 2$, $A^* = 0.1, \beta = 0.2$, $\chi = 0.5$, $Gr = 0.1, Gc = 0.1$, $Ec = 0.2$ and $R = 0.1$

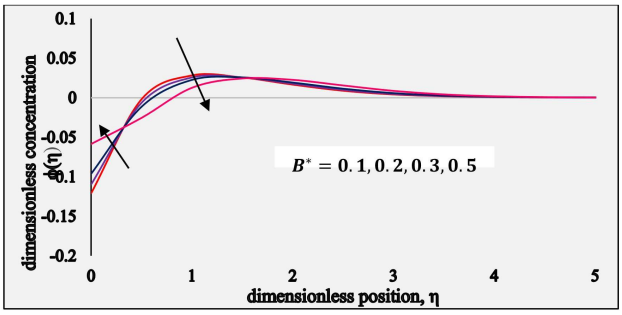

Figure 24: Dimensionless concentration vs B^* when $M = 2.5$, $Pr = 2$, $Nb = Nt = 0.5, Le = 5$, $Bi = 5$, $Pr = 2$, $A^* = 0.1, \beta = 0.2$, $\chi = 0.5$, $Gr = 0.1, Gc = 0.1$, $Ec = 0.2$ and $R = 0.1$

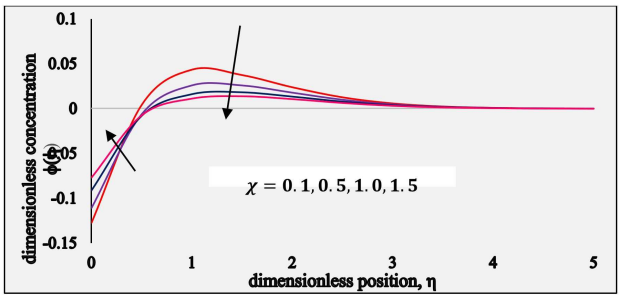

Figure 25: Dimensionless concentration vs χ when $M = 2.5$, $Pr = 2$, $Nb = Nt = 0.5, Le = 5$, $Bi = 5$, $Pr = 2$, $A^* = 0.1, B^* = 0.2$, $\beta = 0.2$, $Gr = 0.1, Gc = 0.1$, $Ec = 0.2$ and $R = 0.1$

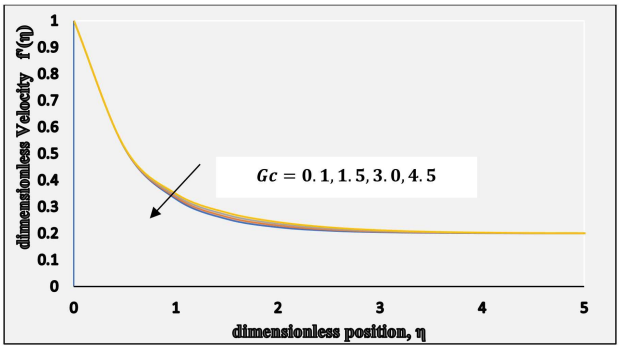

Figure 26: Dimensionless Velocity vs Gc when $M = 2.5$, $Pr = 2$, $Nb = Nt = 0.5, Le = 5$, $Bi = 5$, $Pr = 2$, $A^* = 0.1, B^* = 0.2$, $\beta = 0.2$, $Gr = 0.1, Gc = 0.1$, $Ec = 0.2$ and $R = 0.1$

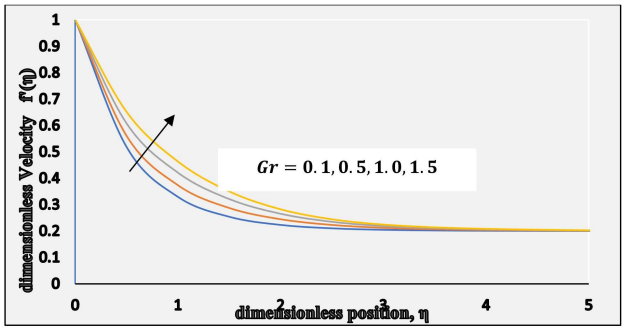

Figure 27: Dimensionless Velocity vs Gr when $M = 2.5$, $Pr = 2$, $Nb = Nt = 0.5, Le = 5$, $Bi = 5$, $Pr = 2$, $A^* = 0.1, B^* = 0.2$, $\beta = 0.2$, $\chi = 0.5, Gc = 0.1$, $Ec = 0.2$ and $R = 0.1$

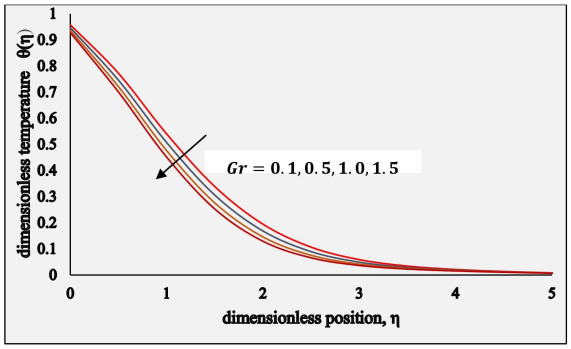

Figure 28: Dimensionless temperature vs Gr when $M = 2.5$, $Pr = 2$, $Nb = Nt = 0.5, Le = 5$, $Bi = 5$, $Pr = 2$, $A^* = 0.1, B^* = 0.2$, $\beta = 0.2$, $\chi = 0.5, Gc = 0.1$, $Ec = 0.2$ and $R = 0.1$

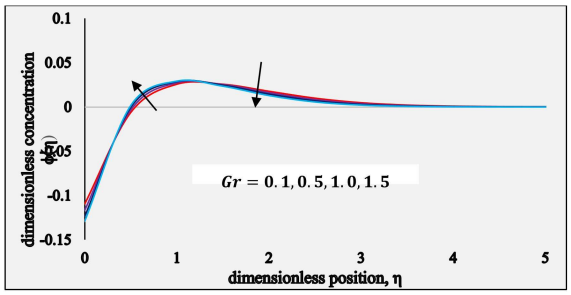

Figure 29: Dimensionless Concentration vs Gr when $M = 2.5$, $Pr = 2$, $Nb = Nt = 0.5, Le = 5$, $Bi = 5$, $Pr = 2$, $A^* = 0.1, B^* = 0.2$, $\beta = 0.2$, $\chi = 0.5, Gc = 0.1$, $Ec = 0.2$ and $R = 0.1$

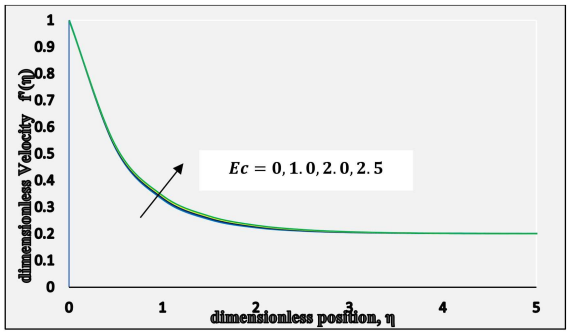

Figure 30: Dimensionless Velocity vs Ec when $M = 2.5$, $Pr = 2$, $Nb = Nt = 0.5, Le = 5$, $Bi = 5$, $Pr = 2$, $A^* = 0.1, B^* = 0.2$, $\beta = 0.2$, $\chi = 0.5, Gc = 0.1$, $Gr = 0.1$ and $R = 0.1$

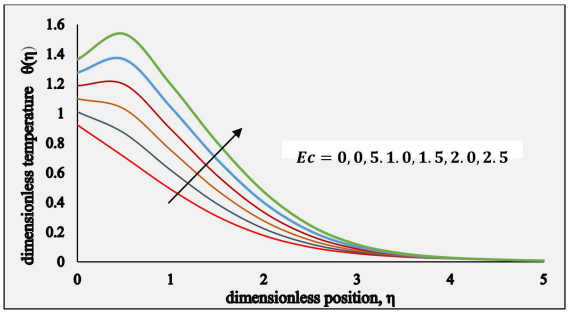

Figure 31: Dimensionless Temperature vs Ec when $M = 2.5$, $Pr = 2$, $Nb = Nt = 0.5, Le = 5$, $Bi = 5$, $Pr = 2$, $A^* = 0.1, B^* = 0.2$, $\beta = 0.2$, $\chi = 0.5, Gc = 0.1$, $Gr = 0.1$ and $R = 0.1$

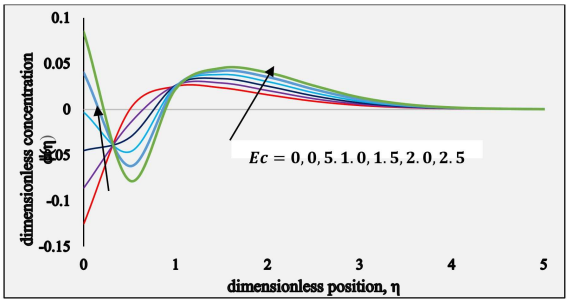

Figure 32: Dimensionless Concentration vs Ec when $M = 2.5$, $Pr = 2$, $Nb = Nt = 0.5, Le = 5$, $Bi = 5$, $Pr = 2$, $A^* = 0.1, B^* = 0.2$, $\beta = 0.2$, $\chi = 0.5, Gc = 0.1$, $Gr = 0.1$ and $R = 0.1$

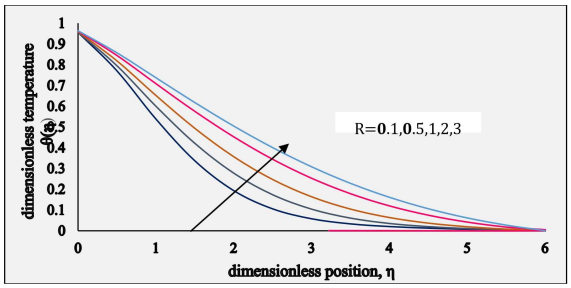

Figure 33: Dimensionless Temperature vs R when $A = 0.2$, $M = 2.5$, $Pr = 2$, $Nt = Nb = 0.5$, $Le = 5, Bi = 5$, $\beta = 0.2$, $A^* = 0.1, B^* = 0.2$, $\chi = 0.5$, $Gr = 0.1, Gc = 0.1$, and $Ec = 0.2$

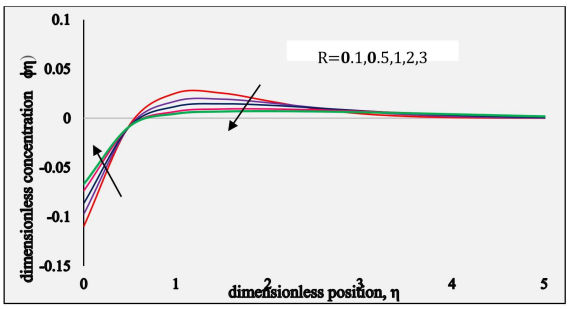

Figure 34: Dimensionless concentration vs R when $A = 0.2$, $M = 2.5$, $Pr = 2$, $Nt = Nb = 0.5$, $Le = 5, Bi = 5$, $\beta = 0.2$, $A^* = 0.1, B^* = 0.2$, $\chi = 0.5$, $Gr = 0.1, Gc = 0.1$, and $Ec = 0.2$

6. Conclusion

After a thorough investigation, we have reached the following concluding observation.

1. The velocity profile increases by increasing A but the temperature and concentration profiles decrease by increasing A.
2. The magnetic parameter M has the same increasing influence on the temperature and the concentration field but opposite on the velocity field.
3. The velocity field f' and the temperature field θ increase by increasing the value of Nt and Bi, but concentration field ϕ decreases for both the parameters.
4. The Lewis number Le has an increasing effect on the velocity field f' temperature field θ and concentration field ϕ.
5. The viscoelastic parameter β has an increasing effect on the velocity profile but decreasing on the temperature and concentration profiles.

6. The space dependent heat generation/absorption coefficient A^* and the temperature dependent heat generation/absorption coefficient B^* have an increasing effect on the velocity field f', temperature field θ and concentration field ϕ.
7. The temperature and concentration fields increase by enlarging the chemical reaction parameter but the velocity field decreases.
8. The velocity f' and the concentration field ϕ increase by enhancing the solutal Grashof number Gc and thermal Grashof number Gr but it causes a decrease in the temperature field.
9. Temperature field $\theta(\eta)$ increases with an increase in thermal radiation R whereas it is observed that concentration decreasing.

Acknowledgment

The authors would like to thanks to **Prof. Koneru S.R.**, Retired Professor, Department of Mathematics, IIT Bombay for his support throughout this research work.

References

[1] S. U. S. Choi, *Enhancing thermal conductivity of fluids with nanoparticles*, ASME-Publications-Fed. 231 (1995) 99–106.
[2] J. Buongiorno, *Convective transport in nanofluids*, J. Heat Trans. 128 (3) (2006) 240–250.
[3] A. V. Kuznetsov and D. A. Nield, *Natural convective boundary-layer flow of a nanofluid past a vertical plate*, Int. J. Thermal Sci. 49(2) (2010) 243–247.
[4] W. A. Khan and I. Pop, *Flow and heat transfer over a continuously moving at plate in a porous medium*, J. Heat Trans. 133(5) (2011) 054501.
[5] L. Zheng, C. Zhang, X. Zhang, and J. Zhang, *Flow and radiation heat transfer of a nanofluid over a stretching sheet with velocity slip and temperature jump in porous medium*, J. Franklin Inst. 350(5) (2013) 990–1007.
[6] H. S. Takhar, R. S. R. Gorla, and V. M. Soundalgekar, *Short communication radiation effects on MHD free convection flow of a gas past a semi-infinite vertical plate*, Int. J. Numerical Meth. Heat Fluid Flow, 6(2) (1996) 77–83.
[7] A. Y. Ghaly and M. E. E. Elsayed, *Radiation effect on MHD free-convection flow of a gas at a stretching surface with a uniform free stream*, J. Appl. Math. 2(2) (2002) 93-103.
[8] S. P. A. Devi and M. Kayalvizhi, *Analytical solution of MHD flow with radiation over a stretching sheet embedded in a porous medium*, Int. J. Appl. Math. Mech. 6(7) (2010) 82-106.
[9] O. D. Makinde, W. A. Khan, and Z. H. Khan. *Buoyancy effects on MHD stagnation point flow and heat transfer of a nanofluid past a convectively heated stretching/shrinking sheet*, Int. J. Heat Mass Trans.62 (2013) 526–533.
[10] H. I. Andersson, *MHD flow of a viscoelastic fluid past a stretching surface*, Acta Mech. 5(1) (1992) 227–230.
[11] M. I. Char, *Heat and mass transfer in a hydromagnetic flow of the viscoelastic fluid over a stretching sheet*, J. Math. Anal. Appl. 186(3) (1994) 674–689.
[12] H. Markovitz and B. D. Coleman, *Incompressible second-order fluids*, Adv. Appl. Mech. 8 (1964) 69–101.
[13] K. R. Rajagopal, *A note on unsteady unidirectional flows of a non-newtonian fluid*, Int. J. Non-Linear Mech. 17(5-6) (1982) 369–373.
[14] K. R. Rajagopal and A. S. Gupta. *An exact solution for the flow of a non-newtonian fluid past an infinite porous plate*, Mecc. 19(2) (1984) 158–160.
[15] A. M. Siddiqui, P. N. Kaloni and O. P. Chandna, *Hodograph transformation methods in non-Newtonian fluids*, J. Engin. Math. 19(3) (1985) 203–216.
[16] A. M. Siddiqui and P. N. Kaloni, *Certain inverse solutions of a non-newtonian fluid*, Int. J. Non-linear Mech. 21(6) (1986) 459–473.
[17] O. P. Chandna and P. V. Nguyen, *Hodograph method in non-Newtonian MHD transverse fluid flows*, J. Engin. Math. 23(2) (1989) 119–139.
[18] P. V. Nguyen and O. P. Chandna, *Non-Newtonian MHD orthogonal steady plane fluid flows*, Int. J. Engin. Sci. 30(4) (1992) 443–453.
[19] R. Cortell, *Heat transfer in a fluid through a porous medium over a permeable stretching surface with thermal radiation and variable thermal conductivity*, Canadian J. Chemical Engin. 90(5) (2012) 1347–1355.

[20] D. P. Bhatta, S. R. Mishra and J. K. Dash, *Unsteady squeezing flow of water-based nanofluid between two parallel disks with slip effects: Analytical approach*, Heat Trans. Asian Res. 48(5) (2019) 1575–1594.

[21] M. Farooq, S. Ahmad, M. Javed and A. Anjum, *Melting heat transfer in squeezed nanofluid flow through Darcy Forchheimer medium*, J. Heat Trans. 141(1) (2019) 012402.

[22] M. Gholinia, K. Hosseinzadeh, H. Mehrzadi, D. Ganji and A. Ranjbar, *Investigation of MHD Eyring Powell fluid flow over a rotating disk under effect of homogeneous-heterogeneous reactions*, Case Stud. Thermal Engin. 13 (2019) 100356.

[23] G.Narender, G.Sreedhar Sarma and K.Govardhan, *Heat and Mass Transfer of a nanofluid over a stretching sheet with viscous dissipation effect*, J. Heat Mass Trans. Res. 6(2) (2019) 117–124.

[24] W. Ibrahim and R. U. Haq. *Magnetohydrodynamic (MHD) stagnation point flow of nanofluid past a stretching sheet with convective boundary condition*, J. Brazilian Soc. Mech. Sci. Engin. 38(4) (2016) 1155–1164.